Electrochemical Na Insertion and Solid Electrolyte Interphase for Hard-Carbon Electrodes and Application to Na-Ion Batteries

Shinichi Komaba, Wataru Murata, Toru Ishikawa, Naoaki Yabuuchi, Tomoaki Ozeki, Tetsuri Nakayama, Atsushi Ogata, Kazuma Gotoh, and Kazuya Fujiwara*

Recently, lithium-ion batteries have been attracting more interest for use in automotive applications. Lithium resources are confirmed to be unevenly distributed in South America, and the cost of the lithium raw materials has roughly doubled from the first practical application in 1991 to the present and is increasing due to global demand for lithium-ion accumulators. Since the electrochemical equivalent and standard potential of sodium are the most advantageous after lithium, sodium based energy storage is of great interest to realize lithium-free high energy and high voltage batteries. However, to the best of our knowledge, there have been no successful reports on electrochemical sodium insertion materials for battery applications; the major challenge is the negative electrode and its passivation. In this study, we achieve high capacity and excellent reversibility sodium-insertion performance of hard-carbon and layered $NaNi_{0.5}Mn_{0.5}O_2$ electrodes in propylene carbonate electrolyte solutions. The structural change and passivation for hard-carbon are investigated to study the reversible sodium insertion. The 3-volt secondary Na-ion battery possessing environmental and cost friendliness, Na^+-shuttlecock hard-carbon/$NaNi_{0.5}Mn_{0.5}O_2$ cell, demonstrates steady cycling performance as next generation secondary batteries and an alternative to Li-ion batteries.

1. Introduction

Lithium-ion batteries play a vital role in our daily life as they are the prominent power sources for cell phones, laptop computers, digital cameras, power tools, electrical assist bicycles, and many consumer products. Recently, lithium-ion batteries have also been attracting more interest for use in automotive and stationary applications. In the next few years, large-scale batteries would be more popular for electric vehicles. At the present time, lithium resources are confirmed to be unevenly distributed in South America. The cost of the lithium raw materials has roughly doubled from the first practical application in 1991 to the present, and it may drastically increase when the demand of lithium increases through commercialization of the large-scale lithium-ion accumulators for automotive applications in the near future.

There is no doubt that the sodium resources are inexhaustible and unlimited everywhere around the world. The electrochemical equivalent and standard potential of sodium are the most advantageous for aprotic battery applications after lithium. However, only a limited number of successful reports are found for sodium insertion of layered Na_xMeO_2 (Me = transition element) materials compared to that for Li_xMeO_2.[1–3] Recently, we investigated the electrochemical performance of layered $NaMeO_2$.[4,5] It is generally known that a graphite electrode is electrochemically inactive as a sodium insertion host in a Na salt electrolyte. Disordered carbon electrodes were previously investigated as the negative electrode in sodium-ion batteries. For example, the initial capacities were 300 mAh g^{-1} by Stevens and Dahn[6] and 285 mAh g^{-1} by Alcántara et al.,[7] but their cycleability was insufficient for the application in Na-ion batteries. The electrochemical cycling of hard-carbon at 60 °C for only ten cycles was investigated in a $NaClO_4$ ethylene carbonate (EC) solution.[8] To the best of our knowledge, there are no reports of passivation and interface analyses of the negative electrodes in Na-ion cell.

It is thought that the first sodium-ion rocking chair cell operating at 100 °C, C/(solid polymer electrolyte)/$Na_{0.6}CoO_2$ configuration, was described by Doeff et al.,[9] and there is another report on the cycleability of the sodium-ion cell, the hard-carbon/($NaClO_4$ EC:dimethyl carbonate (DMC))/$NaVPO_4F$ delivering less than 50% of the original discharge capacity after more than 30 cycles by Barker and co-workers.[10] In this study,

---

Prof. S. Komaba, W. Murata, T. Ishikawa, Prof. N. Yabuuchi, T. Ozeki,
T. Nakayama, Dr. A. Ogata
Department of Applied Chemistry
Tokyo University of Science
1-3 Kagurazaka, Shinjuku, Tokyo 162-8601, Japan
Fax: +81 3 5228 8749
E-mail: komaba@rs.kagu.tus.ac.jp
Prof. K. Gotoh, K. Fujiwara
Department of Chemistry
Okayama University
3-1-1 Tsushima-naka, Kita, Okayama 700-8530, Japan
Fax: +81 86 251 7776S
E-mail: kgotoh@cc.okayama-u.ac.jp

DOI: 10.1002/adfm.201100854

we achieved the high capacity sodium insertion performance of hard-carbon and layered $NaNi_{0.5}Mn_{0.5}O_2$ electrodes, and fabricated hard-carbon/$NaNi_{0.5}Mn_{0.5}O_2$ cells, i.e., secondary Na-ion batteries. The structural change, passivation, and interface structure of hard-carbon are investigated to analyze the sodium insertion mechanism. The unprecedented 3-volt Na-ion battery with environmentally and cost friendly materials demonstrated steady cycling performance and is expected to be an alternative to secondary Li-ion batteries.

2. Negative Electrode and Electrolyte Materials

Considering the previous reports of the lithium insertion into various carbons, we selected two typical ordered and disordered carbons, i.e., graphite and hard-carbon (non-graphitizable carbon), respectively, to test the Na insertion in aprotic electrolyte solutions. In the case of the graphite electrode, the reversible capacity was negligible (Figure S1 in Supporting Information). This is consistent with the general consensus that the electrochemical sodium intercalation into graphite hardly occurs under moderate conditions.[11] On the contrary, the hard-carbon electrode showed a high reversible capacity of 220 mAh g^{-1}. The capacity was, however, gradually reduced by the galvanostatic cycling in the $NaClO_4$ EC:DMC.

For the improvement of the cycle performance, carbonate esters were examined as an electrolyte solvent for the Na cells. First, we investigated the performance of the hard-carbon electrode in cyclic alkylene carbonate solutions. The electrochemical cycling was carried out in the EC, propylene carbonate (PC), and butylene carbonate (BC) electrolyte solutions containing $NaClO_4$ as shown in **Figure 1**. The potentiogram sloped from 1.2 to 0.1 V during the initial reduction, followed by a long flat region between ca. 0.1 and 0 V vs. Na, reaching 250–300 mAh g^{-1}. During the following oxidation, the capacity of 100–130 mAh g^{-1} was observed near 0 V vs. Na/Na^+, and then the potential gradually varied up to 1.2 V, suggesting that hard-carbon underwent reversible sodium insertion. The hard-carbon electrode in the BC electrolyte showed a reversible capacity higher than 230 mAh g^{-1} in the early cycles; however, the serious degradation began after the twentieth cycle. In contrast to the BC solution, the hard-carbon electrode showed a steady capacity retention in the EC and PC solution.

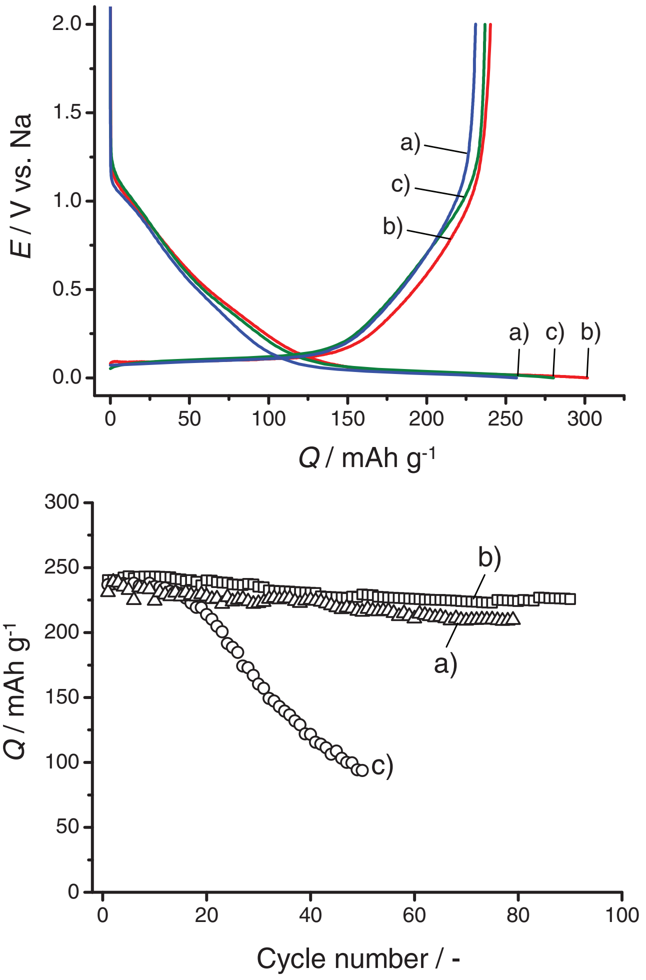

Figure 1. Initial current reversal chronopotentiograms (upper) and variation in reversible capacities (lower) for hard-carbon electrodes in a) EC, b) PC, and c) BC solution containing 1 mol dm^{-3} $NaClO_4$ tested at 25 mA g^{-1} in beaker-type cells.

Second, we tested the hard-carbon electrodes in the binary solvent electrolyte based on EC and linear carbonate esters. In **Figure 2**, the chronopotentiogram in EC:DMC confirms an additional reduction capacity around 0.5–0.2 V which suggests the severe decomposition of DMC. In this system, the cycle performance is constantly deteriorated from the early cycles. In the case of EC:ethyl methyl carbonate (EMC), the irreversible decomposition around 0.5–0.2 V was suppressed. The cycle performance was, however, insufficient. When the EC:diethyl carbonate (DEC) solution was used, the hard-carbon electrode exhibited a high capacity of ca. 240 mAh g^{-1} with a stable capacity retention over 100 cycles and a higher initial coulombic efficiency of 78%.

After several cycles, we visually confirmed that the EC:DEC electrolyte solution was not colored, and no significant change in the FT-IR spectra of the electrolyte was observed. On the other hand, the transparent and colorless electrolyte solution of EC:DMC and EC:EMC was confirmed to be colored in yellow (note that sodium ethoxide and sodium ethyl carbonate are yellow in color), and the formation of sodium alkoxide and/or sodium alkyl carbonate was confirmed by the FT-IR measurements, which would be due to the electrochemical decomposition of the carbonate esters. When the hard-carbon electrodes were also tested in the PC-based electrolyte solutions mixed with DMC, EMC, or DEC, they showed electrochemical activity; however, severe degradation of the activity was observed in all electrolyte solutions (Figure S2). The FT-IR measurement proved the formation of sodium alkoxide and/or sodium alkyl carbonate, indicating a similar decomposition during cycling.

The film-forming additives in the electrolyte are well known to improve the performance of the lithium-ion battery,[12,13] and vinylene carbonate (VC) is commonly accepted as a suitable additive to modify the interface of the electrodes; therefore, the PC and PC:VC (49:1 in volume) solutions were compared in the Na cells. The VC addition, however, results in a negative effect

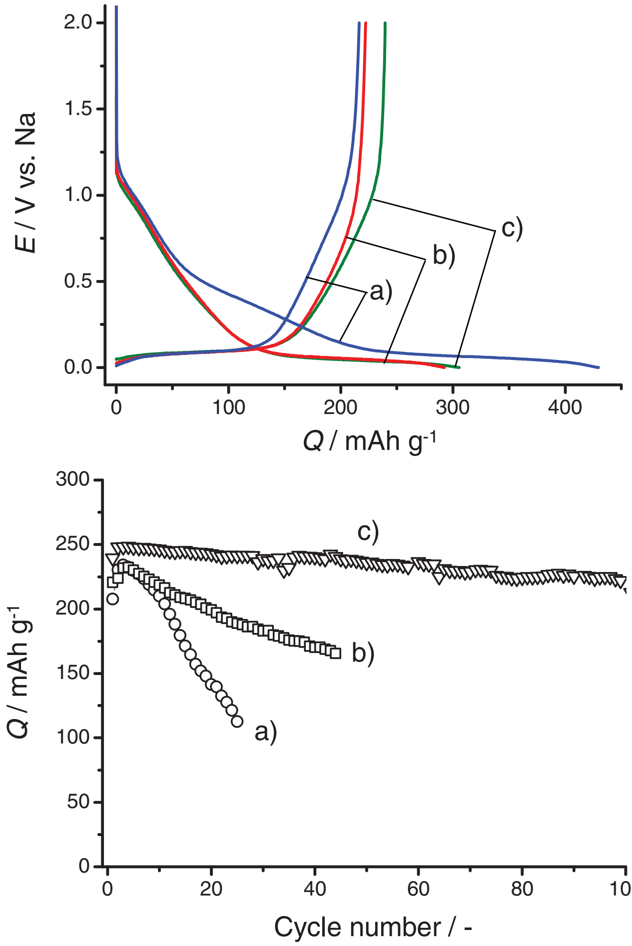

Figure 2. Initial current reversal chronopotentiograms (upper) and variation in reversible capacities (lower) for hard-carbon electrodes in a) EC:DMC (1:1), b) EC:EMC (1:1), and c) EC:DEC (1:1) solution containing 1 mol dm^{-3} NaClO$_4$ at 25 mA g^{-1} in beaker-type cells.

on the Na insertion into the hard-carbon electrodes (Figure S3). This indicates that a different approach is required for the interfacial control for Na insertion electrodes.

As a result, the PC, EC, and EC:DEC solutions enable the hard-carbon electrodes to demonstrate excellent electrochemical performance; highly reversible capacity and excellent capacity retention. Considering the poor low temperature performance due to the high melting point of EC (~37 °C), the PC electrolyte is advantageous for application to Na-ion cells. The ionic conductivities of 1 mol dm^{-3} LiClO$_4$ and NaClO$_4$ PC solutions at 25 °C are 5.2×10^{-3} and 6.6×10^{-3} S cm^{-1}, respectively. As it is generally known that solvation of dissolved Na$^+$ ion is weaker than that of Li$^+$ ion because of lower charge density of larger the Na$^+$ ion, we expect the faster transport of Na$^+$ ions than Li$^+$ ions in the PC solution.

When the hard-carbon electrodes were galvanostatically tested in a coin-type cell instead of the beaker-type cell, we confirmed the similar reversible capacities in the PC electrolyte. Due to the lower irreversibility at the initial cycle, the initial efficiency in the coin-type cell reaches 90%, which is higher than that in the beaker-type cell, 80% (see Figure S4). We believe that this is due to the different cell configuration, that is, the more uniform current distribution at the electrode would lead to a lower irreversibility, similar to that observed for the lithium cell.[12,13] Additionally, not only Cu foil but also Al foil are can be used as current collectors for the hard-carbon electrodes in the Na cells without any problems because there is no apparent electrochemical formation of Na–Cu and Na–Al alloys, unlike lithium-ion batteries.

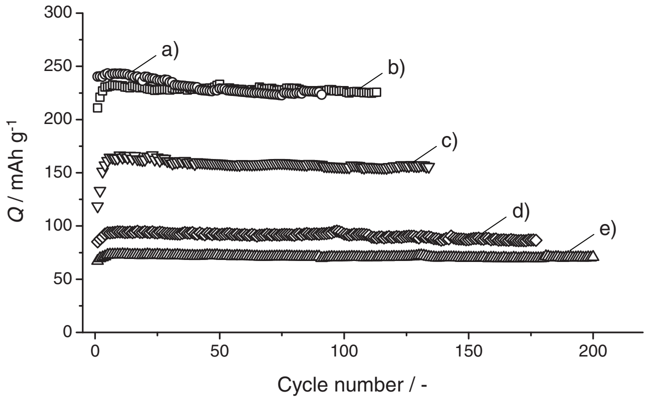

Figure 3. Variation in reversible oxidative capacities at the voltage range from 2.00 V to a) 0.00 V, b) 0.01 V, c) 0.05 V, d) 0.10 V, and e) 0.20 V vs. Na for hard-carbon electrodes in 1 mol dm^{-3} NaClO$_4$ PC at 25 mA g^{-1} in beaker-type cells.

Figure 3 shows the dependence of the reversible capacity on voltage domains, corresponding to the depth of the charge. In the range of 2.00–0.00 V, the highest reversible capacity of ca. 240 mAh g^{-1} was achieved in the successive cycles, and a slight reduction in capacity to 220 mAh g^{-1} was observed during 100 cycles. Even though the initial reversible capacity slightly decreases to ca. 230 mAh g^{-1} in the limited domain of 2.00–0.01 V, degradation of the capacity was not observed over 120 cycles. When the reversible capacity was limited by restricting the voltage domain above 0.05, 0.10, and 0.20 V vs. Na, no capacity degradation was observed during 200 cycles. It is reasonable to think that the improvement relates to the stability of the electrolyte solution at a lower potential. It is concluded that the selection of active material and electrolyte solution is indispensable to achieve a highly stable cycling of negative electrodes for Na-ion batteries.

3. Structural Change and Solid Electrolyte Interphase for Hard-Carbon Electrode

Hard-carbon has been applied in practical Li-ion batteries and the lithium insertion into hard-carbon was studied by many researchers.[14–16] Therefore, we compared the insertion and removal properties of sodium with those of lithium to discuss the Na insertion mechanism.

Chronopotentiograms at the second reduction for hard-carbons examined in 1 mol dm^{-3} NaClO$_4$ or LiClO$_4$ PC electrolytes are shown in **Figure 4**. Although comparable insertion capacities were obtained in both the electrolytes, the features depended on the kinds of alkali elements. In the case of lithium, the sloping curve with higher capacity appeared in the wider potential range between 0 and 1.2 V, and an ambiguous plateau appeared

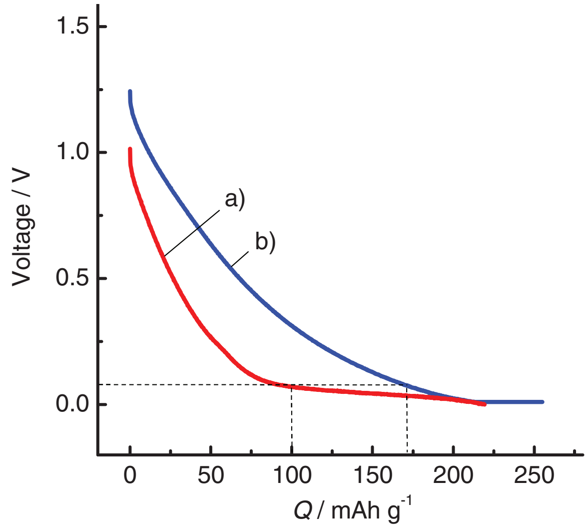

Figure 4. Chronopotentiograms of the second reduction for hard-carbon electrodes in a) 1 mol dm^{-3} NaClO$_4$ and b) 1 mol dm^{-3} LiClO$_4$ PC solution in Na and Li cells, respectively, at a rate of 25 mA g^{-1}. For the Li cell, constant voltage of 0.00 V was applied after reaching 0.00 V.

in the lower potential region near 0 V. For the sodium system, a clear and long plateau was observed around 0.1 V. According to the previous reports,[14–16] lithium insertion between graphene layers and into nanopore of hard-carbon occurs in the sloping and plateau regions, respectively.

To analyze the structural change during the sodium insertion into hard-carbon, we carried out the ex situ X-ray diffraction (XRD) measurements (**Figure 5** upper). For the pristine electrode, the broad Bragg peak centered at $2\theta = 23.4°$ is assigned to the parallel stacking of graphene sheets of hard-carbon. Generally, hard carbons tend to be highly disordered, so that the X-ray diffractive intensity is low and broad. When the hard-carbon electrode was reduced at 0.2 V, the broad peak shifted to a lower angle at 2θ = ca. 21–22°, indicating that the interlayer spacing between the graphene sheets was expanded. This is due to the sodium insertion between the parallel graphene layers, similar to that in lithium cell.[14,15] Simultaneously, the decrease in diffraction intensity is observed because X-ray scattering of inserted sodium between the stacked graphenes. It is believed that larger interlayer spacing (d = ca. 3.8 Å) and/or the smaller crystallite size of the parallel graphenes within hard-carbon in comparison to those of the graphite ($d = 3.354$ Å) are responsible for the sodium insertion. To test this hypothesis in more detail, we need to carry out further experimental studies. After the following oxidation to 2.00 V, the peak returned to the same position to that of the pristine, indicating the reversible Na removal process from the graphene sheets. The variation of the average interlayer distance estimated from XRD patterns is compared for Na and Li insertion in Figure 5 lower. The distance steadily increases as a function of the capacity in the sloped region. In the case of sodium, the rapid elongation of interlayer distance associated with the larger atomic size of sodium is observed. The apparent slope of the spacing vs. capacity plots by lithium insertion into hard-carbon was identical to the average variation for lithium–graphite intercalation compound.[17] Subsequently, the elongated space should become almost constant in the plateau region near 0 V after ca. 100 and 170 mAh g^{-1} in Na and Li cases, respectively (see Figure 4), implying that a different insertion mechanism of sodium exists in the lower voltage domain.

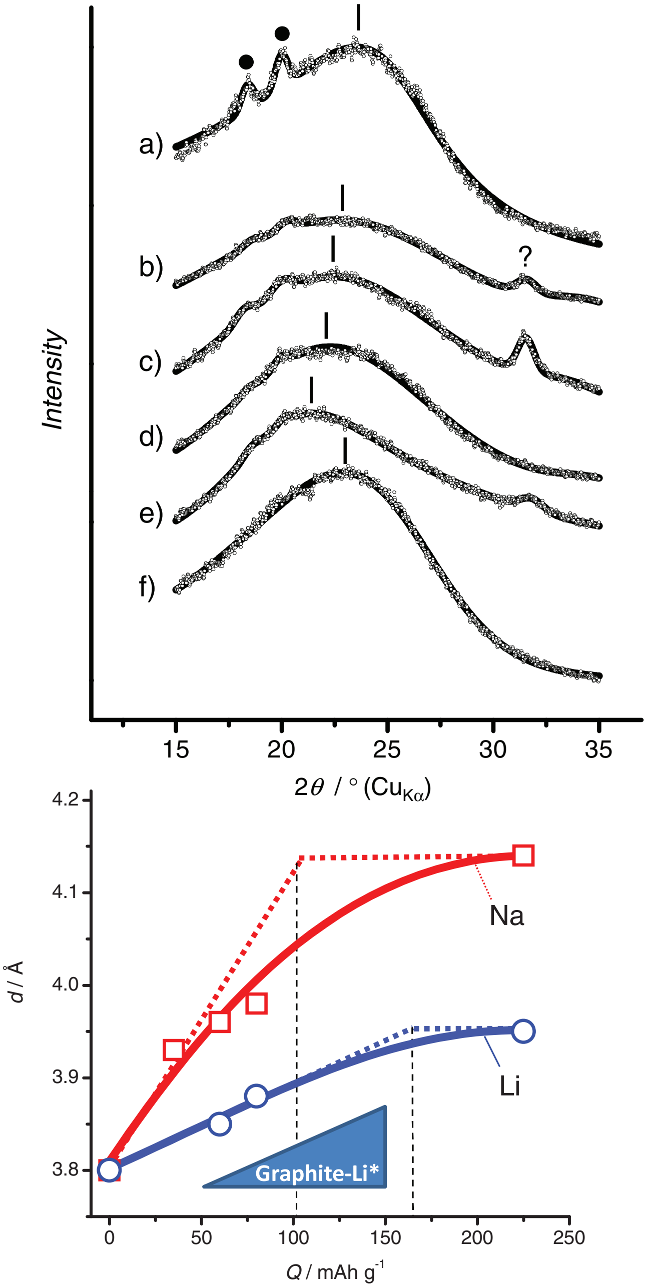

Figure 5. Upper Panel: Ex situ XRD patterns for hard-carbon electrodes: a) pristine electrode, galvanostically reduced to b) 0.40 V, c) 0.20 V d) 0.10 V, e) 0.00 V, and f) oxidized to 2.00 V after reduction to 0.00 V in 1 mol dm^{-3} NaClO$_4$ PC. (• PVdF binder, ? unknown). Lower Panel: Dependence of interlayer spacing estimated from XRD data on insertion capacity for hard-carbon electrodes tested in Na and Li cell. (*Inset triangle shows the mean slope for lithium intercalated graphite from previous data.[17])

Figure 6 shows the ex situ small-angle X-ray scattering (SAXS) patterns. Since the scatter varies with the difference of electron density between the carbon matrix and the inside nanopore,

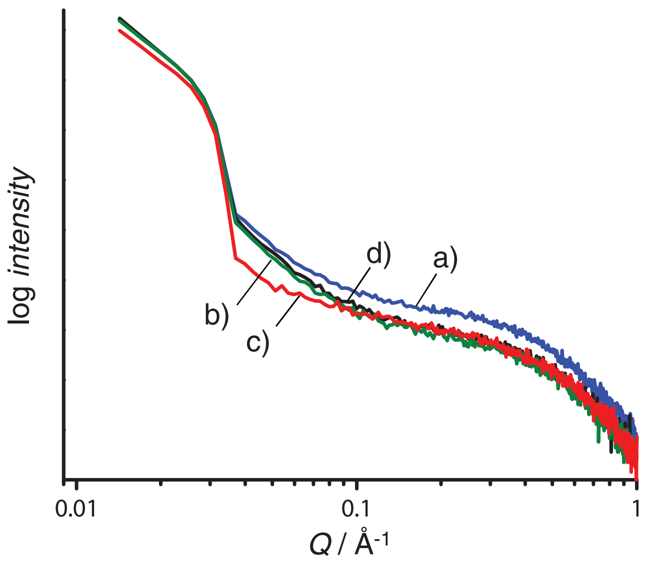

Figure 6. Ex situ SAXS patterns for hard-carbon electrodes: a) pristine, galvanostically reduced to b) 0.20 V and c) 0.00 V, and d) reoxidized to 2.00 V in 1 mol dm^{-3} $NaClO_4$ PC.

SAXS is a useful tool to investigate the nanopore structure of the carbon.[18] When the hard-carbon electrode was electrochemically reduced from 0.20 to 0.00 V, the scattering intensity around 0.03–0.07 Å^{-1}, which was assigned to the nanopores in hard-carbon with a diameter estimated to be ca. 14 Å, decreased reversibly, indicating a decrease in the electron density contrast between the carbon matrix and nanopores. This should be attributed to the reversible sodium insertion into the nanopores.

We examined Raman spectroscopy for Li and Na inserted hard-carbon (Figure S5). According to Hardwick's report,[16] negatively charged graphenes with Li^+ insertion into hard-carbon result in occupation of electron in the π* antibonding-band leading to weakening of the C–C bond, resulting in the elongation of the C–C bond length and, therefore, subsequent red-shift of the G-band. From our Raman data, we observed the identical red-shift during Li and Na insertion into hard-carbon during the voltage-sloping region (Figure S5). After the potential approaches to 0 V (> 100 and > 170 mAh g^{-1} in Li and Na cells, respectively), Raman peak of G-band does not shift in both cells, indicating that the state of negatively charged graphenes does not change in the lower potential region. In the case of Li insertion, a nano-sized cluster of quasimetallic Li is formed in the nanopore of hard-cabon.[14,19] To prove the Na insertion mechanism undoubtedly, state analyses of sodium inserted into hard-carbon are under progress by means of nuclear magnetic resonance and X-ray photoelectron spectroscopy.

The XRD, SAXS, and Raman data demonstrate the structural change of hard-carbon, indicating the reversible Na insertion into disordered stacked graphenes and nanopores of hard-carbon. Consequently, at least two different mechanisms of electrochemical sodium insertion exist for hard-carbon, and these results agree well with the previous report.[6] In the galvanostatic curves in the Li and Na cells (see Figure 4), the sloping region between 1.2 and 0.2 V was assigned to the alkali insertion between the graphene sheets, and the higher capacity is observed in the Li cell. The insertion into the nanopores is of significance for the Na system compared to the Li system.

Generally, almost all polar organic solvents including PC are not thermodynamically stable at ~0 V vs. Na; therefore, passivation must play a key role in cycle performance of sodium insertion into hard-carbon. Currently, there is much knowledge on passivation for electrodes in a Li-ion cell, the so-called solid electrolyte interphase (SEI); therefore, we carried out a comparative investigation of passivating surfaces for hard-carbons in Na and Li cells.

We observed the morphology of the hard-carbons cycled in the Li and Na cells by SEM (Figure S6). It confirmed that the small particles of a sub-micrometer size were dispersed on the electrode surface in both cells and were probably formed by electrochemical decomposition of the electrolyte solutions. In the Na cell, the particles were larger in size and unevenly distributed compared to the Li cell. From the TEM observation in Figure S7, a surface film with a thickness of approximately 30 nm in dry conditions certainly exists on the tested hard-carbon, and the morphology of the surface films was different in both cases. That is, in the case of Na, the rough and nonuniform deposit layer was observed on the surface. On the other hand, the uniform layer covered the surface in the Li cell.

The X-ray photoelectron spectroscopy (XPS) measurements reveal the difference of the surface layers formed by the electrochemical cycling. In **Figure 7**, a strong peak at 284.5 eV in the spectra was assigned to the sp^2 carbon in C–C of graphene

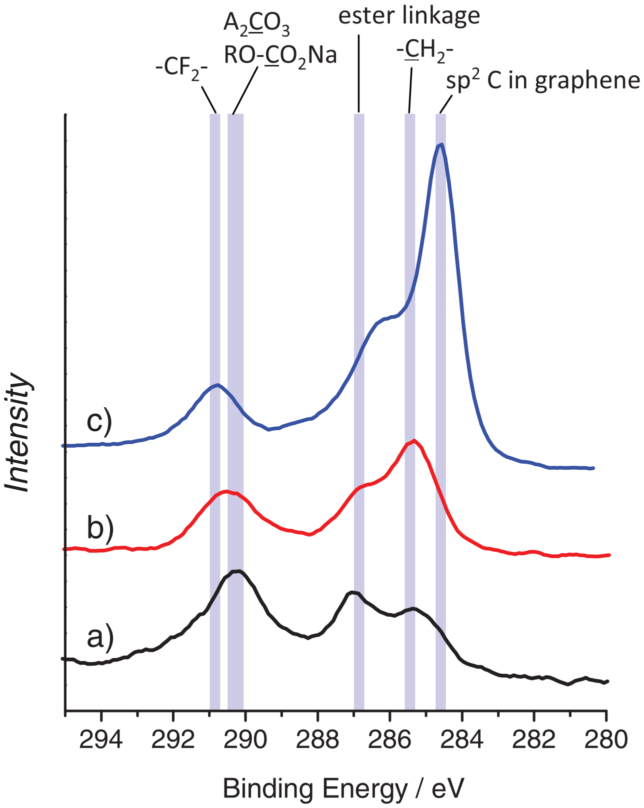

Figure 7. XPS carbon 1s spectra for the hard-carbon electrodes tested in a) sodium and b) lithium cells after the first cycle, and c) pristine electrode.

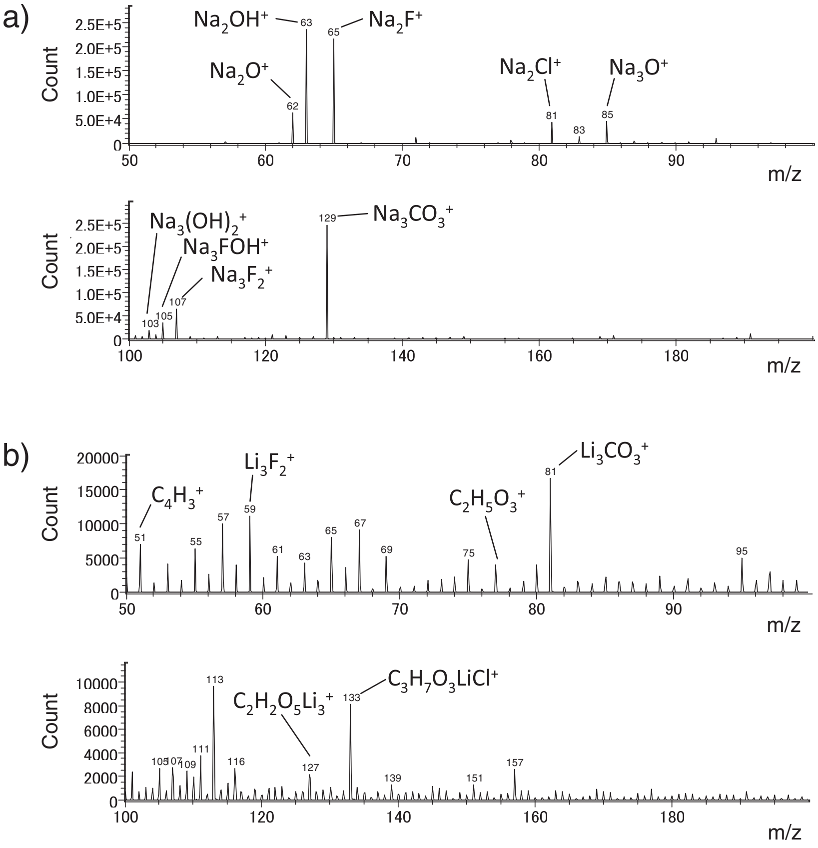

Figure 8. TOF-SIMS positive ion spectra for the hard-carbon electrodes after the first galvanostatic cycle in a) sodium and b) lithium cells.

of hard-carbon. The other peaks originated from the PVdF binder (–CF_2– at 290.8 eV) and various functional groups on the hard-carbon electrodes.[20,21] After the electrochemical tests, the peak at 284.5 eV almost disappeared, indicating that hard-carbon in both cells is covered with the decomposition products of the electrolyte as seen by SEM and TEM. The peaks were assigned to various compounds such as alkali carbonate of A_2CO_3 (A = Li or Na) and alkyl carbonate of $ROCO_2A$ at 290.0–290.5 eV, ester linkage (–CO–O–) at 286.8 eV, and –CH_2– at 285.5 eV. The apparent difference of two electrodes was observed in 285.5 eV; that is, the peak intensity in –CH_2– is stronger for the Li cell than that in the Na cell. Since –CH_2– originated from the alkyl and alkylene groups and polymer species,[22] the larger amount of hydrocarbon compounds was found in the surface film formed in the Li cell as is also evidenced below by time-of-flight secondary ion mass spectroscopy (TOF-SIMS).

The XPS oxygen 1s spectra (Figure S8) also support the existence of A_2CO_3 and $ROCO_2A$, corresponding to a peak at 532 eV. The peak with the binding energy of 533.7 eV, which was assigned to oxygen in alkoxides generated by the decomposition of solvent, appears more clearly in case of the Na cell. When Ar^+ etching progresses, the peak intensity of O 1s in the Na cell decreases more rapidly than that in the Li cell; simultaneously, the peak of sp^2 carbon became more clear and intense in the C 1s spectra, indicating that the surface layer in the Na cell is thinner than that in the Li cell. Furthermore, the peak shape of the XPS O 1s spectra similarly changes for both cases by Ar^+ etching, suggesting a similar depth distribution of the chemical species. In the SEI of the Li-ion cells, the organic compounds of alkoxide, alkyl carbonate, and polymers and the inorganic compounds of A_2CO_3 and A_2O are distributed in the shallow and deep part of the layer, respectively, as previously reported.[23,24] The distribution exists for the Na-ion cell from the XPS results.

The difference of the surface film components is evidenced by TOF-SIMS as shown in **Figure 8**. In the Na cell, small numbers of fragment peaks are observed, and their intensity is markedly higher in comparison with that of the Li cell, and the fragments were mainly assigned to the inorganic fragment components such as m/z = 62 (Na_2O^+), 63 (Na_2OH^+), 65 (Na_2F^+), 81 (Na_2Cl^+), 85 (Na_3O^+), 107 ($Na_3F_2^+$), and 129 ($Na_3CO_3^+$). On the contrary, a large number of fragments at every m/z = 1 were observed in the Li cell, and most of them were assigned to organic fragments, for instance, m/z = 51 ($C_4H_3^+$), 77 ($C_2H_5O_3^+$), 127 ($C_2H_2O_5Li_3^+$), 133 ($C_3H_7O_3LiCl^+$), with inorganics of m/z = 59 ($Li_3F_2^+$) and 81 ($Li_3CO_3^+$). These results prove that the surface film in the Li cell was mainly composed of the organic compounds while that in sodium was composed of the inorganic compounds. Moshkovich et al. pointed out the higher stability of the surface species formed in the $LiClO_4$ PC than that in the $NaClO_4$ PC.[25] The above results confirm that a passivation layer different from the lithium-based negative electrode exists for the sodium-based electrode. It might be related to the different nature of lithium and sodium, such as ionic size, cationic solvation, reactivity, solubility and so on.

As is generally accepted, many organic solvents including carbonate esters are not thermodynamically stable at the standard potential of Na; therefore, the interfacial passivation is essentially required for long-term cycling. To examine the passivation property of the fully Na-inserted hard-carbon, we carried out self-discharge tests of the hard-carbon electrodes after full Na and Li insertion at the tenth cycle as seen in **Figure 9**. There is a negligible self-discharge since the discharge capacity is approximately 80% after a month, and a similar trend in both Na and Li cells is confirmed. This result indicates that the surface film works as a passivation film, which similarly protects the sodium and lithium inserted hard-carbon from the chemical reactions with the electrolyte at interface, whereas the morphology and chemical composition of the surface film are different in both cases.

As broadly accepted, the thin surface layer of SEI is formed on the negative electrode in the Li-ion cells. The concept of SEI was first introduced by Peled.[26] According to Peled's literature, alkali and alkali-earth metals are always covered by a surface layer, and SEI should meet the following terms: i) this surface layer protects a direct and free contact between the electrode and

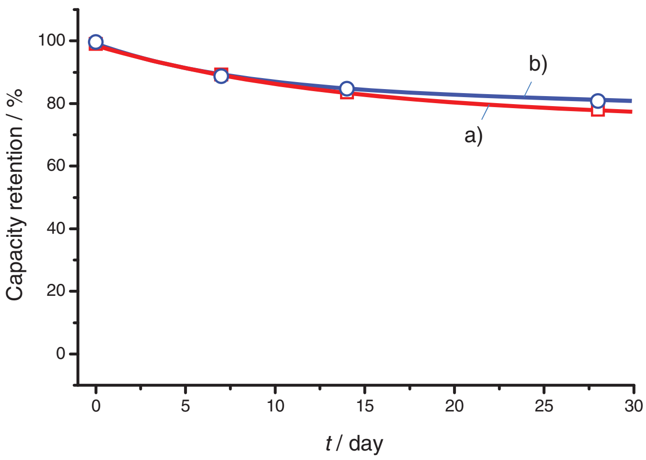

Figure 9. Capacity retention of the hard-carbon electrodes after full insertion of a) sodium and b) lithium at the tenth cycle.

the solution and ii) electrons are not allowed to pass through the interphase (the SEI is a pure cationic conductor). When we consider these definitions for the hard-carbon electrode in the Na cell, the former definition was proved in the study of SEM, TEM, XPS, and TOF-SIMS, and the latter definition was confirmed by the electrochemical cycling and self-discharge tests. Therefore, we conclude that the SEI layer allows for the reversible Na insertion of the hard-carbon. The morphology and chemical composition of the SEI are different for the Na and Li cases even though we use the same electrode and electrolyte material except for intercalant alkali element. Further investigation of the formation process and ionic conductivity for the SEI layer in the sodium-ion containing electrolyte is in progress and will be reported elsewhere.

4. Full Cell Performance of Na-Ion Batteries

We recently studied the positive electrode materials of layered $NaNi_{0.5}Mn_{0.5}O_2$ and $NaCrO_2$ (space group: *R*-3*m*).[4,5] The $NaNi_{0.5}Mn_{0.5}O_2$ electrode exhibits the high reversible capacity due to the reversible sodium deintercalation with $Ni^{2/3/4+}$ redox. As shown in **Figure 10**, the stable cycle performance was achieved with a highly reversible capacity of 125 mAh g^{-1} in a $Na/NaNi_{0.5}Mn_{0.5}O_2$ cell between 2.0 and 3.8 V. There appear to be several potential plateaux in the charge and discharge curves which are due to the reversible phase transition by the sliding of $Ni_{0.5}Mn_{0.5}O_2$ slabs and Na^+/vacancy ordering.[4]

Based upon the Na-insertion electrodes, we fabricated and tested the coin-type full Na-ion (shuttlecock) batteries consisting of the $NaNi_{0.5}Mn_{0.5}O_2$ positive and the hard-carbon negative electrodes (**Scheme 1**) with PC solutions containing 1 mol dm^{-3} $NaClO_4$, $NaPF_6$, and $NaN(SO_2CF_3)_2$ (sodium bis(trifluoromethanesulfonyl)amide, NaTFSA). Although all systems showed a high reversible capacity >200 mAh g^{-1} (negative electrode basis) during the initial cycles, a decrease in the reversible capacity was observed in the $NaClO_4$ system (Figure S9). In contrast, the hard-cabon/$NaNi_{0.5}Mn_{0.5}O_2$ cells with the $NaPF_6$ and NaTFSA solutions exhibited a superior cycle performance, and the capacity retention after fifty cycles was >70% although the Al is corrosive in a TFSA solution. After the electrochemical tests in the $NaClO_4$ solution, we disassembled the coin-type cells and then visually confirmed that the separator loaded with the electrolyte solution was colored yellow, whereas no change in color of the separator was observed for the $NaPF_6$ and NaTFSA. The FT-IR measurement confirmed the sodium alkoxide and/or sodium alkyl carbonate contained in the colored separator. This phenomenon indicates that the $NaClO_4$ dissolved PC electrolyte was not sufficiently stable for the long term cycling of Na-ion batteries.

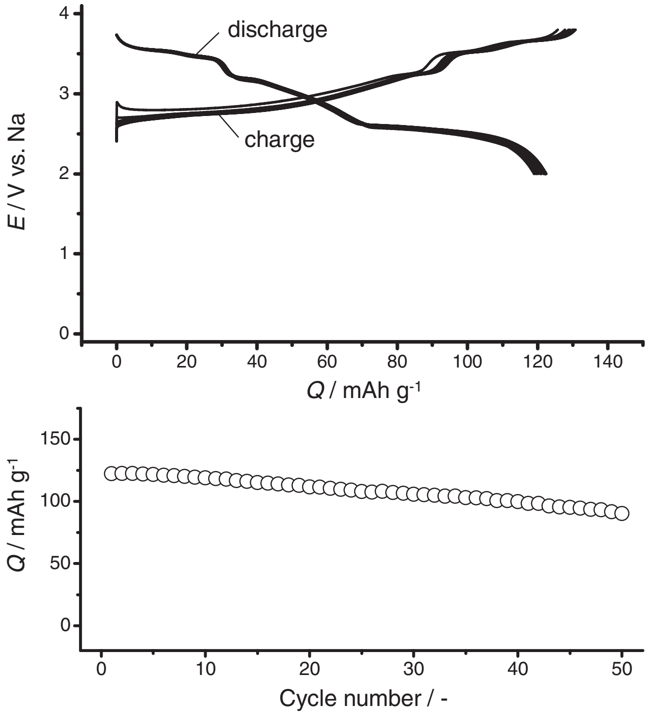

Figure 10. (upper) Galvanostatic charge and discharge curves for a beaker-type $Na/NaNi_{0.5}Mn_{0.5}O_2$ cell filled with 1 mol dm^{-3} $NaClO_4$ PC solution at 24 mA g^{-1} and (lower) the variation in discharge capacity.

Figure 11 shows the electrochemical performance of a hard-cabon/$NaNi_{0.5}Mn_{0.5}O_2$ cell at room temperature. The hard-cabon/$NaNi_{0.5}Mn_{0.5}O_2$ cell exhibited a high capacity more than 200 mAh g^{-1} (negative electrode basis) and an average

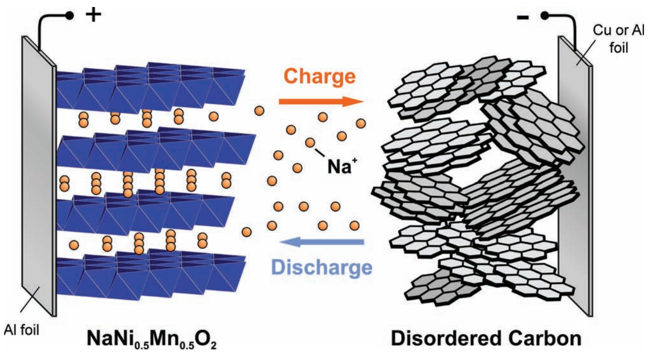

Scheme 1. The rocking chair type Na-ion battery.

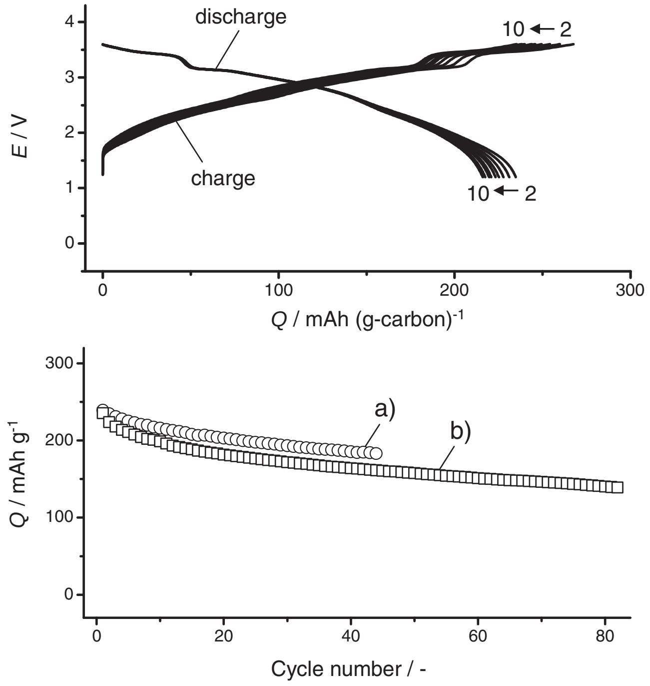

Figure 11. (upper) Charge and discharge curves of a coin-type hard-carbon/$NaNi_{0.5}Mn_{0.5}O_2$ battery with 1 mol dm^{-3} NaTFSA PC at 25 mA g^{-1}, and (lower) the discharge capacity variation tested at a) 25 and b) 300 mA (g-carbon)$^{-1}$.

operating voltage of ca. 3 V. Several voltage plateaus, which are ascribed to the $NaNi_{0.5}Mn_{0.5}O_2$ electrode, are distinguishable in the charge–discharge curves. To the best of our knowledge, this is the first report on the satisfactory cycle performance of the Na-ion battery. The energy density of the Na-ion battery is compared with that of the conventional Li-ion battery by assuming the available capacities and average voltage as follows: 3.7 volt Li-ion cell of $LiCoO_2$ (140 mAh g^{-1})/graphite (350 mAh g^{-1}) and 2.8 volt Na-ion cell of $NaNi_{0.5}Mn_{0.5}O_2$ (120 mAh g^{-1})/hard-carbon (240 mAh g^{-1}) without consideration of battery package and irreversible capacity. As a result, the Na-ion battery in this study achieves ca. 60% of the practical energy density of the conventional Li-ion battery. Furthermore, when the Na-ion cell was tested at a higher rate of 300 mA g^{-1}, no significant decrease in capacity is observed, indicating that the hard-cabon/$NaNi_{0.5}Mn_{0.5}O_2$ cell demonstrates a remarkable rate capability (Figure 11 lower). When the battery was tested at an elevated temperature of 60 °C, a similar cycle performance to that at room temperature was obtained over 50 cycles without any additional degradation (Figure S10). The kinetics of Na^+ ion transportation in the electrode and electrolyte and solvation/desolvation of Na^+ ions at the interface are under investigation to understand the dependence of the battery performance on current rate and high temperature.

5. Conclusions

The excellent performance of hard-carbon and $NaNi_{0.5}Mn_{0.5}O_2$ as active materials was achieved for the advanced Na-ion batteries. The combination of positive and negative electrodes, solvent, and electrolyte salt with a sufficient purity is important to achieve the highly stable cycling of the Na-ion batteries. We believe that the new concepts of insertion materials and interface design at the electrode/electrolyte, including new additives,[12,13,27] binders,[28–30] and so on, will be developed to realize the higher performance of Na-ion batteries. Not only new electrode materials but also solvents, sodium salts, current collector, etc., should be thoroughly studied, and their combination must be optimized for practical applications, reminiscent of the history of lithium-ion batteries over the past 40 years. The Na^+ shuttlecock battery with environmentally and cost friendly materials, which is free from rare metals, has high potential as a possible alternative to lithium-ion batteries in the future.

6. Experimental Section

Materials: The reagent grade artificial graphite (KS-10, Sigma-Aldrich Co.), metallic sodium, and poly(vinylidene fluoride) (PVdF) (Wako Pure Chemical Industries, Ltd.) were used. Battery grade lithium foil (Honjo Metal Co., Ltd.), ethylene carbonate (EC), propylene carbonate (PC), butylene carbonate (BC), dimethyl carbonate (DMC), ethyl methyl carbonate (EMC), diethyl carbonate (DEC), vinylene carbonate (VC), $LiClO_4$, $NaClO_4$ (containing ca. 100 ppm H_2O), $NaPF_6$, $NaN(SO_2CF_3)_2$ (all solvents and salts are battery grade purchased from Kishida Chemical Co., Ltd.), and commercially available hard-carbon (Carbotron P(J), Kureha Co., its characterization was described in[19]) were used without any further purification and treatment. All chemicals were handled in an Ar-filled glove box to avoid air exposure and contamination. The $NaNi_{0.5}Mn_{0.5}O_2$ was synthesized by calcination of a pelletized mixture of coprecipitated $Ni_{0.5}Mn_{0.5}(OH)_2$ and Na_2CO_3 powders at 800 °C in air for 24 h.[4]

Electrochemical Characterization: For preparation of the negative electrodes, the hard-carbon or the graphite powders (90 wt%) were mixed with PVdF as a binder (10 wt%) in *N*-methylpyrrolidinone. The obtained slurry was pasted onto a nickel mesh or doctor-bladed onto Cu or Al foil. For preparation of the positive electrodes, the $NaNi_{0.5}Mn_{0.5}O_2$ (80 wt%) and acethylene black (10 wt%) were mixed with PVdF (10 wt%) in *N*-methylpyrrolidinone. The obtained black slurry was pasted onto a stainless mesh or doctor-bladed onto Al foil. The electrodes were dried at >80 °C in a vacuum prior to use. The beaker-type electrochemical cells consisted of the carbon or $NaNi_{0.5}Mn_{0.5}O_2$ as a working electrode, lithium or sodium foil as the quasi reference electrode, and electrolyte solutions, which were assembled with special care for reproducibility and negligible polarization. The coin-type cells (20 mm diameter, 3.2 mm thickness) with hard-carbon, $NaNi_{0.5}Mn_{0.5}O_2$, electrolyte, and a glass fiber filter (Toyo Roshi Kaisha, Ltd.) as a separator were fabricated. These cells were assembled in an Ar filled glove-box (dew point < –70 °C). The cyclic voltammetry was performed in a three-electrode configuration with a Li/Li^+ or Na/Na^+ reference electrode. The electrochemical tests were carried out at room temperature around 25 °C or elevated temperature (60 °C).

Materials Characterization: The X-ray diffraction (XRD) patterns were collected using Multiflex (Rigaku Co., Ltd., Japan) with Cu Kα radiation at 40 kV and 30 mA. The small angle X-ray scattering (SAXS) patterns were collected with SmartLab (Rigaku Co., Ltd., Japan) with Cu Kα radiation at 45 kV and 200 mA. The tested electrodes were observed by scanning electron microscope (SEM, S-5000, Hitachi) and transmission electron microscope (TEM, 200 kV, H-9500, Hitachi). The X-ray photoelectron spectroscopy (XPS, JPS-9010MC, JEOL) was employed using monochromatic Al Kα as the incident X-rays, and depth profiling was made by argon ion beam sputtering. The time-of-flight secondary ion mass spectroscopy (TOF-SIMS, PHI TRIFT V, ULVAC-PHI) operated with Bi_3^{2+} source and pulse electron flooding. During the analysis, the targets were bombarded by the 30 keV Bi_3^{2+} beams with a pulsed primary ion current varying at 0.047 pA.

Supporting Information

Supporting Information is available from the Wiley Online Library or from the author.

Acknowledgements

The authors would like to thank Dr. A. Nagai, Kureha Co., for supplying the hard-carbon products. This study was supported by NEDO, NSG Foundation for Materials Science and Engineering, and KAKENHI (No. 21750194), and the Funding Program for Next Generation World-Leading Researchers, JSPS, Japan.

Received: April 18, 2011

[1] C. Delmas, J.-J. Branconnier, C. Fouassier, P. Hagenmuller, *Solid State Ionics* **1981**, *3-4*, 165–169.
[2] T. Shirane, R. Kanno, Y. Kawamoto, Y. Takeda, M. Takano, T. Kamiyama, F. Izumi, *Solid State Ionics* **1995**, *79*, 227–233.
[3] S. Okada, Y. Takahashi, T. Kiyabu, T. Doi, J. Yamaki, T. Nishida, *Meet. Abstr. - Electrochem. Soc.* **2006**, *602*, 201–201.
[4] S. Komaba, T. Nakayama, A. Ogata, T. Shimizu, C. Takei, S. Takada, A. Hokura, I. Nakai, *ECS Trans.* **2009**, *16*, 43–56.
[5] S. Komaba, C. Takei, T. Nakayama, A. Ogata, N. Yabuuchi, *Electrochem. Commun.* **2010**, *12*, 355–358.
[6] D. A. Stevens, J. R. Dahn, *J. Electrochem. Soc.* **2000**, *147*, 1271–1273.
[7] R. Alcántara, P. Lavela, G. F. Ortiz, J. L. Tirado, *Electrochem. Solid-State Lett.* **2005**, *8*, A222–A225
[8] P. Thomas, D. Billaud, *Electrochim. Acta* **2002**, *47*, 3303–3307.
[9] M. M. Doeff, Y. Ma, S. J. Visco, L. C. De Jonghe, *J. Electrochem. Soc.* **1993**, *140*, L169–L170.
[10] J. Barker, M. Y. Saidi, J. L. Swoyer, *Electrochem. Solid-State Lett.* **2003**, *6*, A1–A4.
[11] Y. Mizutani, T. Abe, M. Inaba, Z. Ogumi, *Synth. Methods* **2002**, *125*, 153–159.
[12] S. Komaba, T. Itabashi, T. Ohtsuka, H. Groult, N. Kumagai, B. Kaplan, H. Yashiro, *J. Electrochem. Soc.* **2005**, *152*, A937–A946.
[13] S. Komaba, T. Itabashi, M. Watanabe, H. Groult, N. Kumagai, *J. Electrochem. Soc.* **2007**, *154*, A322–A330.
[14] K. Tatsumi, J. Conard, M. Nakahara, S. Menu, P. Lauginie, Y. Sawada, Z. Ogumi, *Chem. Commun.* **1997**, 687–688.
[15] M. Nagao, C. Pltteloud, T. Kamiyama, T. Otomo, K. Itoh, T. Fukunaga, K. Tatsumi, R. Kanno, *J. Electrochem. Soc.* **2006**, *153*, A914–A919.
[16] L. J. Hardwick, P. W. Ruch, M. Hahn, W. Scheifele, R. Kötz, P. Novák, *J. Phys. Chem. Solid*, **2008**, *69*, 1232–1237.
[17] T. Ohzuku, Y. Iwakoshi, K. Sawai, *J. Electrochem. Soc.* **1993**, *140*, 2490–2498.
[18] O. Glatter, O. Kratky, *Small-Angle X-ray Scattering*, Academic Press, New York **1982**.
[19] K. Gotoh, M. Maeda, A. Nagai, A. Goto, M. Tansho, K. Hashi, T. Shimizu, H. Ishida, *J. Power Sources* **2006**, *162*, 1322–1328.
[20] J. S. Gnanaraj, M. D. Levi, E. Levi, G. Salitra, D. Aurbach, John E. Fischer, A. Claye, *J. Electrochem. Soc.* **2001**, *154*, A525–A536.
[21] D. Aurbach, B. Markovsky, I. Weissman, E. Levi, Y. Ein-Eli, *Electrochim. Acta* **1999**, *45*, 67–86.
[22] V. Eshkenazi, E. Peled, L. Burstein, D. Golodnitsky, *Solid State Ionics* **2004**, *170*, 83–91.
[23] E. Peled, D. Golodnitsky, G. Ardel, *J. Electrochem. Soc.* **1997**, *144*, L208–L210.
[24] Y. Ein-Eli, *Electrochem. Solid-State Lett.* **1999**, *2*, 212–214.
[25] M. Moshkovich, Y. Gofer, D. Aurbach, *J. Electrochem. Soc.* **2001**, *148*, E155–E167.
[26] E. Peled, *J. Electrochem. Soc.* **1979**, *126*, 2047–2051.
[27] S. Komaba, in *Advanced Materials and Methods for Lithium-Ion Batteries* (Ed: S. S. Zhang), Transworld Research Network, KeralaIndia **2007**, Chapter *13*, pp.295–319.
[28] S. Komaba, K. Okushi, T. Ozeki, H. Yui, Y. Katayama, T. Miura, T. Saito, H. Groult, *Electrochem. Solid-State Lett.* **2009**, *12*, A107–A1010.
[29] S. Komaba, T. Ozeki, T. Okushi, *J. Power Sources* **2009**, *189*, 197–203.
[30] S. Komaba, S. Shimomura, N. Yabuuchi, T. Ozeki, H. Yui, K. Konno, *J. Phys. Chem. C* **2011**, *115*, 13487–13495.